



Anti- σ^{28} Factor FlgM Regulates Flagellin Gene Expression and Flagellar Polarity of *Treponema denticola*

Kurni Kurniyati,^{a,b} Yunjie Chang,^{c,d} Wangbiao Guo,^{c,d} Jun Liu,^{c,d} Michael G. Malkowski,^e Chunhao Li^{a,b}

^aDepartment of Oral Craniofacial Molecular Biology, Virginia Commonwealth University, Richmond, Virginia, USA

^bDepartment of Microbiology and Immunology, Virginia Commonwealth University, Richmond, Virginia, USA

^cDepartment of Microbial Pathogenesis, Yale University, School of Medicine, New Haven, Connecticut, USA

^dMicrobial Sciences Institute, Yale University, School of Medicine, New Haven, Connecticut, USA

^eDepartment of Structural Biology, Jacobs School of Medicine and Biomedical Sciences, University of Buffalo, Buffalo, New York, USA

ABSTRACT FlgM, an antagonist of FliA (also known as σ^{28}), inhibits transcription of bacterial class 3 flagellar genes. It does so primarily through binding to free σ^{28} to prevent it from forming a complex with core RNA polymerase. We recently identified an FliA homolog (FliA_{Td}) in the oral spirochete *Treponema denticola*; however, its antagonist FlgM remained uncharacterized. Herein, we provide several lines of evidence that TDE0201 functions as an antagonist of FliA_{Td}. TDE0201 is structurally similar to FlgM proteins, although its sequence is not conserved. Heterologous expression of TDE0201 in *Escherichia coli* inhibits its flagellin gene expression and motility. Biochemical and mutational analyses demonstrate that TDE0201 binds to FliA_{Td} and prevents it from binding to the σ^{28} -dependent promoter. Deletions of *flgM* genes typically enhance bacterial class 3 flagellar gene expression; however, deletion of *TDE0201* has an opposite effect (e.g., the mutant has a reduced level of flagellins). Follow-up studies revealed that deletion of *TDE0201* leads to FliA_{Td} turnover, which in turn impairs the expression of flagellin genes. Swimming plate, cell tracking, and cryo-electron tomography analyses further disclosed that deletion of *TDE0201* impairs spirochete motility and alters flagellar number and polarity: i.e., instead of having bipolar flagella, the mutant has flagella only at one end of cells. Collectively, these results indicate that TDE0201 is a FlgM homolog but acts differently from its counterparts in other bacteria.

IMPORTANCE Spirochetes are a group of bacteria that cause several human diseases. A unique aspect of spirochetes is that they have bipolar periplasmic flagella (PFs), which bestow on the spirochetes a unique spiral shape and distinct swimming behaviors. While the structure and function of PFs have been extensively studied in spirochetes, the molecular mechanism that regulates the PFs' morphogenesis and assembly is poorly understood. In this report, FlgM, an anti- σ^{28} factor, is identified and functionally characterized in the oral spirochete *Treponema denticola*. Our results show that FlgM regulates the number and polarity of PFs via a unique mechanism. Identification of FliA and FlgM in *T. denticola* sets a benchmark to investigate their roles in other spirochetes.

KEYWORDS spirochetes, *Treponema*, flagella, sigma factors, anti-sigma factors

Bacterial flagella are complex molecular machines that are important for motility, biofilm formation, and pathogenesis. More than 30 different proteins are coordinately assembled to constitute three distinct parts of the flagella: the basal body (motor), hook (joint), and filament (propeller) (1–3). The basal body is embedded within the cell envelope and works as a reversible rotary motor (4–6). The hook acts as a flexible joint that connects the basal body and filament, a long helical structure composed of tens of thousands of subunits of a single protein called flagellin (7). Flagellin proteins are synthesized in the cytoplasm and exported through the hook-basal body (HBB) (8). To cope with sophisticated flagellar structure, most bacteria have evolved a complex transcriptional hierarchy to control

Editor Michael Y. Galperin, NCBI, NLM, National Institutes of Health

Copyright © 2023 American Society for Microbiology. All Rights Reserved.

Address correspondence to Chunhao Li, cli5@vcu.edu.

The authors declare no conflict of interest.

Received 2 December 2022

Accepted 7 January 2023

Published 30 January 2023

their flagellar gene expression both temporally and spatially (1, 2). Within this regulatory hierarchy, the operons that encode flagellar, motility, and chemotaxis proteins can be divided into three transcriptional classes. Class 1 genes encode FlhC and FlhD, two master regulators that initiate the expression of class 2 genes, which mainly encode HBB structural proteins and two transcriptional regulators, FliA (also called σ^{28}) and FlgM (anti- σ^{28}). As a flagellum-specific alternative σ factor, FliA initiates the expression of class 3 genes, such as those encoding flagellin and chemotaxis proteins. As an antagonist of FliA, FlgM negatively regulates the expression of class 3 genes through direct interaction with FliA, preventing it from forming a complex with core RNA polymerase (RNAP) (9, 10). FlgM can also attack and destabilize the FliA-RNAP holoenzyme and inhibit transcription initiation (11). FlgM exerts its inhibitory role on flagellar gene expression through a partner-switching mechanism in response to HBB assembly and completion (12, 13). Specifically, FlgM and FliA remain bound as a complex in the cytoplasm until HBB assembly is completed, whereupon FlgM is exported out of cells, releasing FliA to initiate transcription of class 3 genes. This regulatory paradigm was first established in the two model organisms *Escherichia coli* and *Salmonella enterica* serovar Typhimurium (1, 2, 13). Later, a similar regulatory scheme was found in numerous motile bacteria, such as *Campylobacter jejuni* (14), *Helicobacter pylori* (15, 16), *Pseudomonas aeruginosa* (17), *Vibrio cholerae* (18), and *Bacillus subtilis* (13, 19). Deletions of *fliA* led to mutants deficient in flagellar filaments and nonmotile, highlighting the gene's essential role in bacterial flagellar synthesis and motility (16, 18, 20–22). In contrast, deletions of *flgM* typically increase class 3 flagellar gene expression: e.g., deletions of the *flgM* gene in *H. pylori* and *S. Typhimurium* enhance flagellin gene expression by several fold (16, 23).

Spirochetes are a group of bacteria that cause several human diseases: e.g., Lyme disease (*Borrelia burgdorferi*), syphilis (*Treponema pallidum*), leptospirosis (*Leptospira interrogans*), and periodontal disease (*Treponema denticola*) (24–27). A unique aspect of spirochetes is that they have bipolar flagella encased within the periplasmic space. Therefore, spirochetal flagella are named endoflagella or periplasmic flagella (PFs) (28, 29). Spirochetes are diverse in terms of flagellar number and length and whether or not PFs overlap at the middle of cells (29). For example, *L. interrogans* has a single short flagellum inserted at each pole that does not overlap the other (30). In contrast, *B. burgdorferi* has 7 to ~11 long PFs subterminally inserted at the cell poles. These PFs form two bundles of ribbon-like structures that overlap at the middle regions of the cells (31, 32). PFs confer upon spirochetes a distinctive flat-wave or spiral morphology and unique form of screw-like motility that empower them to translocate through viscous substrates and tissues to access otherwise inaccessible host niches (29, 33). Therefore, in pathogenic spirochetes, motility facilitates invasion and dissemination and is essential for infection (26, 34). Like external flagellates, PFs are also composed of a motor, hook, and filament; however, they are more complex in terms of motor structures and flagellar filament compositions (35). For example, PFs have a unique structure called the “collar,” a large multiprotein complex consisting of an inner core and an outer turbine-like structure. The collar has a remarkable structural plasticity essential not only for assembly of flagellar motors in the highly curved membrane of spirochetes but also for generation of the high torque necessary for spirochete motility (36–38). The flagellar hook protein FlgE in spirochetes self-catalyzes the formation of an unusual intersubunit lysinoalanine cross-link critical for cell motility (39, 40). Spirochetes are complex in terms of flagellar filament compositions. Most spirochetes have multiple flagellin proteins (28, 29). For instance, the flagellar filaments of *T. denticola* and *T. pallidum* comprise at least one sheath protein, FlaA, and three core FlaB proteins (41–45). The flagellar filament of *Leptospira* is even more complex as it is composed of two FlaA proteins, at least one FlaB protein, and two novel *Leptospira*-specific flagellar filament proteins, FcpA and FcpB (30, 46, 47). It is noteworthy that FlaB proteins are homologs of FliC. FlaA proteins are unique to spirochetes and do not share sequence similarity with bacterial flagellin proteins (28).

While the structure and function of PFs have been extensively studied in spirochetes (29, 30), the molecular mechanism that regulates PFs' morphogenesis is poorly understood. Thus far, it remains unclear if spirochetes have evolved the aforementioned transcriptional hierarchy to regulate flagellar gene expression and assembly. In our recent studies, we

have been seeking to fill this gap by using *T. denticola* as a model organism. Similar to other spirochetes, the flagellar filaments of *T. denticola* are composed of at least one FlaA protein and three FlaB proteins (FlaB1, FlaB2, and FlaB3). The genes encoding these four proteins are regulated by different promoters (41, 44). For instance, a conserved σ^{28} -dependent promoter is mapped upstream of *flaB2*, and a σ^{70} -dependent promoter is mapped upstream of *flaA* and *flaB1* of *T. denticola* (41). Additionally, we recently identified and functionally characterized an FliA homolog (FliA_{Td}) in *T. denticola* and found that it functions as a flagellum-specific σ^{28} factor that positively regulates the flagellin genes of *T. denticola* (48). However, FlgM, an antagonist of FliA, has not been identified in *T. denticola* or other spirochetes. In this report, by using the approaches of bioinformatics, genetics, biochemistry, and cryo-electron tomography (cryo-ET), we provide several lines of evidence that TDE0201 is an FlgM homolog that regulates the flagellin gene expression and flagellar number and polarity of *T. denticola*.

RESULTS AND DISCUSSION

TDE0201 is an FlgM homolog. Our recent study shows that TDE2683 is a FliA (σ^{28}) homolog that regulates the later class 3 flagellar genes of *T. denticola* (48), yet its antagonist FlgM has not been identified. FlgM proteins (PF04316 and PF05998) are not conserved, and their sizes are diverse, ranging from 65 to 131 amino acids (aa) (49). The function of FlgM has been well characterized in *S. Typhimurium*, and its three-dimensional (3D) structure was determined in *Aquifex aeolicus* as a complex with σ^{28} by X-ray crystallography (11, 50, 51). Using these two bacterial FlgM proteins as queries, we searched the genome of *T. denticola* for their homologs and found that TDE0201 has 15.73% shared sequence identity with *S. Typhimurium* FlgM (FlgM_{St}) and 20.48% shared identity with *A. aeolicus* FlgM (FlgM_{Aa}). We also performed large-scale sequence alignment analyses and found that TDE0201 shares a very limited sequence identity to its counterparts from other bacteria out of the *Treponema* genus, indicating that TDE0201 is not conserved. This is also true for other bacterial FlgM homologs: e.g., *H. pylori* FlgM (HP1122) is ~11% identical to the *E. coli* homolog (15). TDE0201 consists of 93 aa, and its predicted molecular weight (MW) is 10.54 kDa. Previous structural studies indicate that both FlgM_{Aa} and FlgM_{St} are composed of four α -helices (H1', H2', H3', and H4') (50, 51). Sequence alignment analysis revealed that, similar to FlgM_{Aa}, TDE0201 also comprises four α -helices, among which H2' and H3' align well and contain several conserved residues (e.g., Val33, Ser36, Leu42, and Ile63), although their overall conservation is relatively low (Fig. 1A). To further determine if TDE0201 is an FlgM homolog, we generated its structural model using chain D from the cocrystal structure of σ^{28} /FlgM_{Aa} complex (PDB code 1rp3) (50) as a template and found that the two proteins share a similar structural architecture and their H3' helices are well aligned (Fig. 1B). The alignment also uncovered significant differences in the positioning of the N-terminal helices, likely due to their disordered nature in the absence of binding to the σ^{28} factors (51). Collectively, sequence alignment and homology modeling analyses suggest that TDE0201 is an FlgM homolog; thus, here, it is denoted FlgM_{Td}.

The *flgM_{Td}* gene is regulated by a σ^{70} -dependent promoter. The *flgM_{Td}* gene (*TDE0201*) and its upstream *TDE0200* gene are in the same transcriptional orientation (Fig. 2A). *TDE0200* encodes a rRNA small subunit methyltransferase I (RsmI) responsible for the 2'-O-methylation of cytidine 1402 in bacterial 16S rRNA (52). Co-reverse transcription-PCR (co-RT-PCR) analysis showed that only the pair of primers bridging *TDE0200* and *TDE0201* yielded a positive band, whereas the other two pairs of primers across the intergenic regions of *TDE0199-TDE0200* and *TDE0201-TDE0202* were both negative (Fig. 2B), suggesting that *TDE0201* is cotranscribed with its upstream *TDE0200* gene but not with its downstream *TDE0199* gene, a gene in an opposite transcriptional direction. By using 5' rapid amplification of cDNA ends (5'-RACE), we identified a transcriptional start site (TSS) at the upstream region of *TDE0200*, 21 bp from its start codon (Fig. 2C). The -10 and -35 regions from the TSS contain a consensus sequence of σ^{70} -dependent promoter (TTGATT-N17-TATAAT) (Fig. 2D), suggesting that the expression of *flgM_{Td}* is most likely controlled by σ^{70} .

FlgM_{Td} inhibits *E. coli* motility and *fliC* expression. FlgM_{Td} shares about 16% sequence identity and a similar structural topology with *E. coli* FlgM (FlgM_{Ec}). We speculated that if

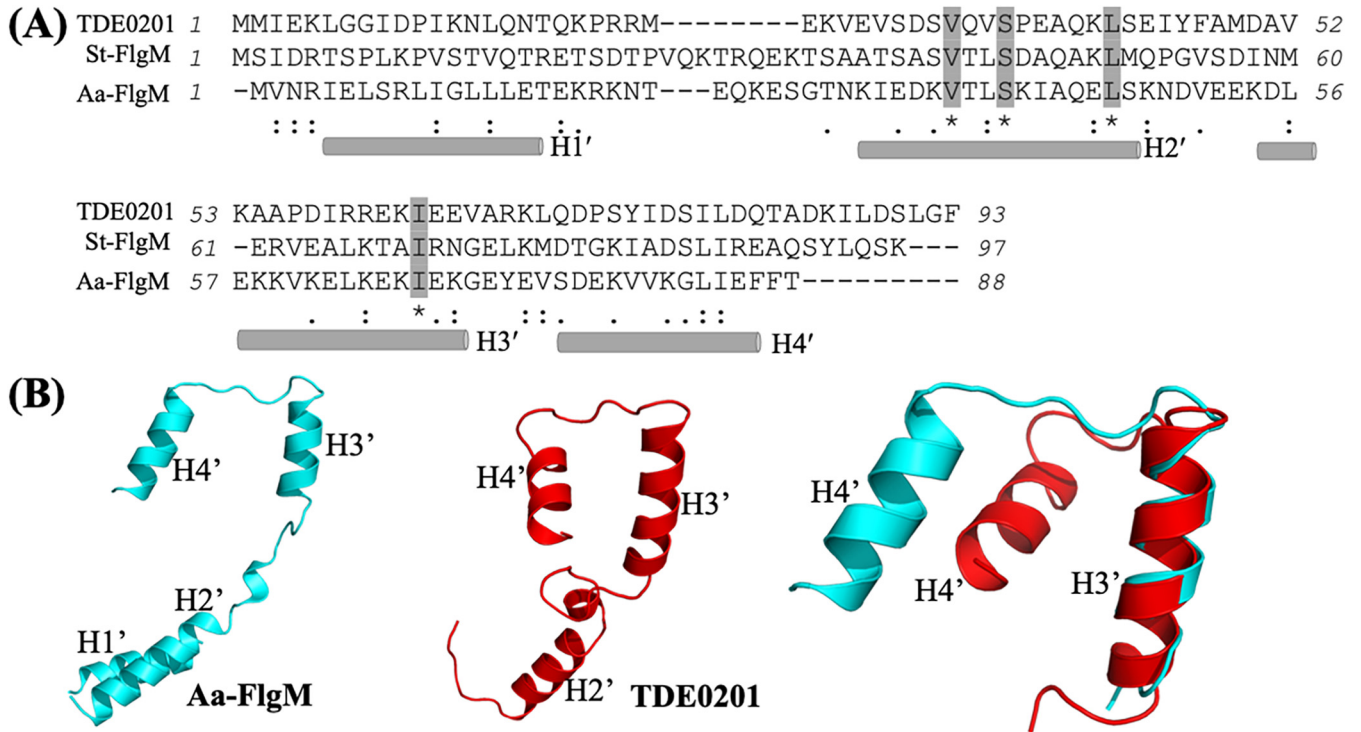


FIG 1 TDE0201 is a homolog of FlgM. (A) Sequence alignment of FlgM homologs. The numbers show the positions of amino acids of *T. denticola* TDE0201 (WP_002666518), *S. Typhimurium* FlgM (St-FlgM) (NP_460143), and *A. aeolicus* FlgM (Aa-FlgM) (WP_010880181.1). The rods represent four helices of FlgM, including H1', H2', H3', and H4'. The alignments were conducted using the program Clustal Omega. (B) Homology modeling of TDE0201. The structural model was generated using chain D from the cocrystal structure of *A. aeolicus* σ^{28} /FlgM complex (PDB code 1rp3) (50) as a template with MODELLER version 10.0 (83) and the MPI Bioinformatics Toolkit (84). The H3' helices of TDE0201 and FlgM_{Aa} were superimposed.

FlgM_{Td} functions as an anti- σ^{28} factor, overexpressing this gene in *E. coli* may impair its late flagellar gene expression (e.g., the flagellin gene *fliC*) and motility. To determine if this is the case, we ectopically expressed *flgM_{Td}* in an *E. coli* DH5 α strain and then assessed its impact on motility using swimming plate assays and the level of FliC using immunoblotting analysis. Supporting our speculation, these two experiments showed that induction of *flgM_{Td}* with IPTG (isopropyl- β -D-1-thiogalactopyranoside) substantially inhibited *E. coli* motility (Fig. 3A) and expression of FliC (Fig. 3B). FlgM proteins are exported when HBB assembly is completed. To determine if FlgM_{Td} can be exported in *E. coli*, after addition of IPTG,

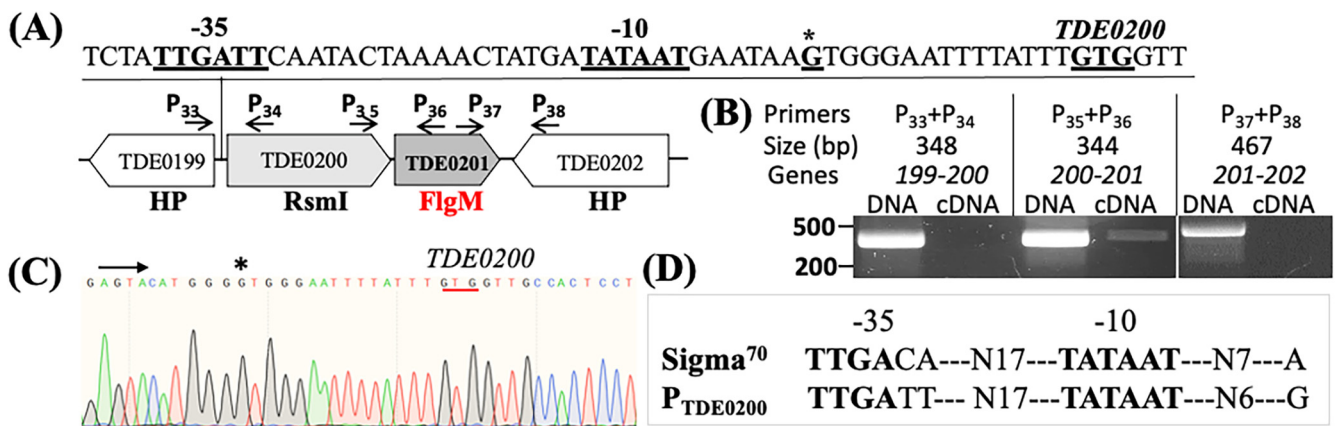


FIG 2 TDE0201 resides in a gene cluster that is regulated by a σ^{70} promoter. (A) Diagram showing the genes adjacent to TDE0201. Arrows represent the relative positions and orientations of RT-PCR primers that span the intergenic regions between individual genes as labeled. (B) RT-PCR analysis. For each pair of primers, chromosomal DNA was used as a positive control. The numbers below the primers are predicted sizes of RT-PCR and PCR products. (C) 5'-RACE analysis. The arrow shows the sequencing direction, and an asterisk indicates the transcriptional start site (TSS). The red underlined sequence (GTG) is the start codon of TDE0200. (D) Sequence comparison between the canonical *E. coli* σ^{70} promoter sequence and that identified upstream of TDE0200.

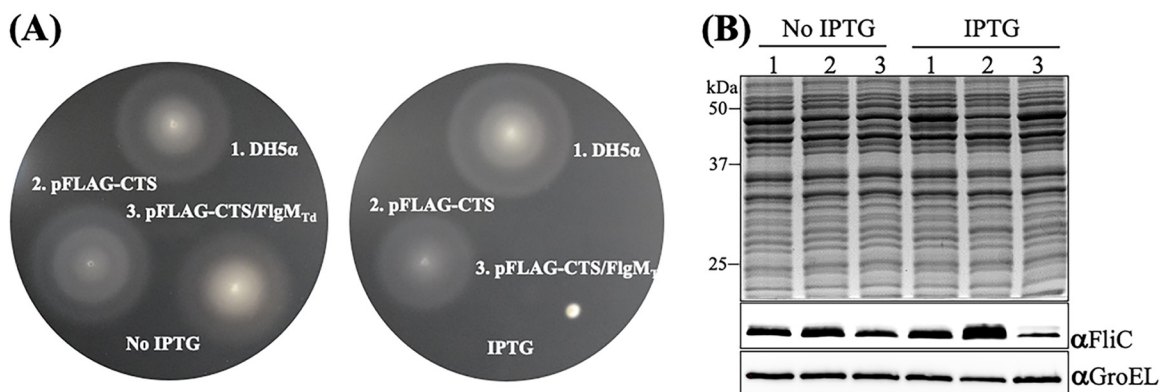


FIG 3 Heterologous expression of *flgM_{Td}* inhibits *E. coli* motility and *fliC* expression. (A) Swimming plate assays with/without IPTG induction. This assay was carried out on agar plates containing 1% tryptone, 0.5% NaCl, and 0.3% Bacto agar as previously documented (86). The plates were incubated at 30°C overnight. Numbers on the plates represent the following conditions: 1, DH5 α alone; 2, DH5 α transformed with the empty vector pFLAG-CTS; and 3, DH5 α transformed with the vector pFLAG-CTS containing *flgM_{Td}*. (B) Detection of FliC by immunoblotting analysis. For this experiment, equivalent amounts ($\sim 10 \mu\text{g}$) of whole-cell lysates of three *E. coli* strains were analyzed by SDS-PAGE and then probed with specific antibodies against *E. coli* GroEL (αGroEL) and FliC (αFliC). GroEL was used as a loading control.

we monitored the presence of FlgM_{Td} in the growth medium of DH5 α by immunoblotting with the FLAG antibody (anti-Flag). We detected FlgM_{Td} in the whole-cell lysates of DH5 α but not in the supernatants concentrated from the growth medium (data not shown), suggesting that no FlgM_{Td} was secreted into the growth medium via the flagellar export apparatus of *E. coli* or that it was secreted but its level in the growth medium was too low to be detected. This result is understandable because the domain essential for FlgM_{Ec} export lies in its N-terminal region (53), which is not conserved in FlgM_{Td} (Fig. 1A). Altogether, the heterologous expression of FlgM_{Td} in *E. coli* indicates that it shares some common characteristics with FlgM_{Ec} (i.e., binding to FliA and repressing flagellin gene expression and motility).

FlgM_{Td} interacts with FliA_{Td}. As an anti- σ^{28} factor, FlgM exerts its inhibitory role on class 3 flagellar gene expression via binding to FliA (11, 13). To determine if FlgM_{Td} interacts with FliA_{Td}, we first conducted protein-protein docking analysis by comparing their homology models, which were generated from the cocrystal structure of the σ^{28} /FlgM complex in *A. aeolicus* (PDB code 1rp3) (50). The docking analysis suggested that FlgM_{Td} binds to FliA_{Td} primarily through its C-terminal H3'-H4' α -helices, whereby H4' is buried in a deep hydrophobic pocket of FliA_{Td} (Fig. 4A). To experimentally test the interaction between FliA_{Td} and FlgM_{Td} *in vivo*, we carried out coimmunoprecipitation (co-IP) assays using *T. denticola* whole-cell lysates and a specific antibody against FliA_{Td} (anti-FliA_{Td}). The resulting samples were then subjected to immunoblotting probed against anti-FlgM_{Td} to determine if FlgM_{Td} was precipitated along with FliA_{Td}. FlgM_{Td} was detected in the eluates from the wild type (WT) but not in those from the $\Delta\textit{flgM}$ mutant (Fig. 4B), suggesting that FlgM_{Td} and FliA_{Td} form a complex; otherwise, it would not have been pulled down by anti-FliA_{Td}. To corroborate this result, we coexpressed His-FliA_{Td} and FlgM_{Td}-FLAG in *E. coli* BL21 cells as previously described (54). After induction with IPTG, two recombinant proteins were copurified under native conditions using FLAG beads. The resulting coeluates were then subjected to SDS-PAGE, followed by immunoblotting probed against either anti-His or anti-Flag antibodies. Our results show that His-FliA_{Td} was copurified along with FlgM_{Td}-FLAG (Fig. 4C and D). Previous structural and mutagenesis studies indicate that FlgM interacts with FliA mainly via its C-terminal H3'-H4' helices, which bind to the $\sigma 4$ domain of FliA (11, 50, 53). To determine if the interaction between FlgM_{Td} and FliA_{Td} is specific, we mutated E221 and V231, two conserved residues in the $\sigma 4$ domain of FliA_{Td} (48), and truncated the H4' helix (79 to 93 aa) of FlgM_{Td}. We first repeated the copurification experiment using three mutated FliA_{Td} proteins (E221D, V231E, and E221D V231E) and found that the single mutation in V231 and double mutations in both E221 and V231 nearly abolished the interaction of two proteins, whereas the mutation in E221 had no impact (Fig. 4C and D). We then repeated this experiment using the

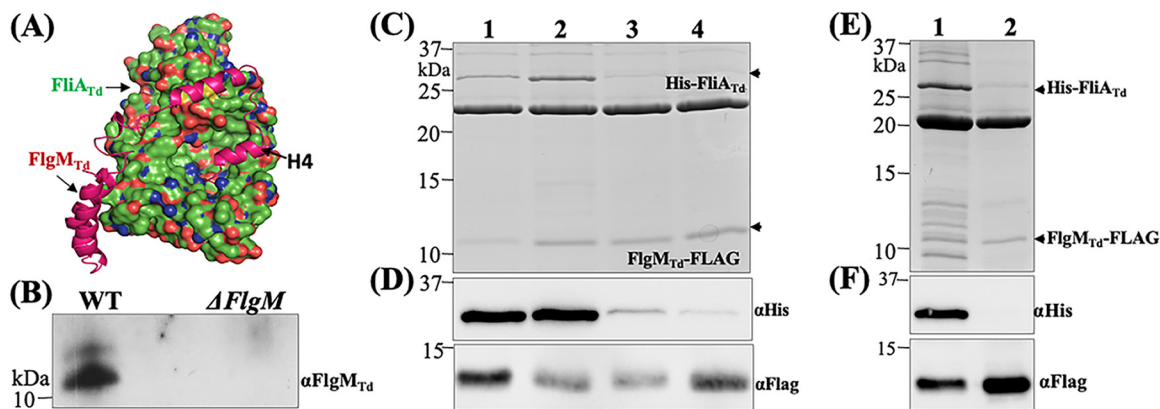


FIG 4 FliA_{Td} interacts with FlgM_{Td}. (A) Protein-protein docking analysis of FliA_{Td} and FlgM_{Td}. The homology models of FliA_{Td} and FlgM_{Td} were first generated using the cocrystal structure of *A. aeolicus* σ^{28} /FlgM complex (PDB code 1rp3), and then protein-protein docking analysis was conducted on the ClusPro server, with FliA_{Td} shown as a molecular surface and FlgM_{Td} shown as a backbone ribbon. (B) Coimmunoprecipitation (co-IP). This assay was performed using *T. denticola* whole-cell lysates and a polyclonal antibody against FliA_{Td} (α FliA_{Td}). The final co-IP eluates were probed using anti-FlgM_{Td}. A deletion mutant of *flgM*_{Td} (Δ *flgM*) was used as a negative control. (C to F) Copurification of N-terminal His-tagged FliA_{Td} (His-FliA_{Td}) and C-terminal FLAG-tagged FlgM_{Td} (FlgM_{Td}-FLAG). The two tagged proteins and their corresponding site-directed mutated or truncated proteins were coexpressed in the *E. coli* BL21 Star(DE3) strain and then purified using FLAG beads. The resulting samples were subjected to SDS-PAGE (C and E), followed by immunoblotting analysis (D and F) using either anti-FLAG (α Flag) or anti-His (α His) antibodies. In panels C and D, in addition to the wild-type FliA_{Td} protein (lane 1), three site-directed mutated recombinant proteins were included: E221D (lane 2), V231E (lane 3), and a double mutation of E221D and V231E (lane 4). In panels E and F, lane 1 shows the wild-type FlgM_{Td} protein and lane 2 shows a truncated FlgM_{Td} protein without the H4' helix (79 to 93 aa).

truncated FlgM_{Td} (Δ H4') and found that the truncation completely abolished the interaction between FlgM_{Td} and FliA_{Td} (Fig. 4E and F). Based on these results, we infer that FlgM_{Td} binds to FliA_{Td} mainly through its C-terminal H4' helix.

FlgM_{Td} prevents FliA_{Td} from binding to the σ^{28} -dependent promoter. Our recent study shows that FliA_{Td} binds to σ^{28} -dependent promoters, such as the *flaB2* promoter (P_{flaB2}) (48). We reasoned that if FlgM_{Td} acts as an anti- σ^{28} factor, it should sequester FliA_{Td} and prevent it from binding to σ^{28} -dependent promoters. To test this hypothesis, we carried out an electrophoretic mobility shift assay (EMSA) using biotin-labeled P_{flaB2} as a DNA probe. Our results showed that the recombinant FliA_{Td} (rFliA_{Td}) bound to P_{flaB2} , which was titrated by the recombinant FlgM_{Td} (rFlgM_{Td}) in a dose-dependent manner (Fig. 5). Notably, rFlgM_{Td} alone did not bind to P_{flaB2} . Along with the above result, we conclude that FlgM_{Td} functions as an anti- σ^{28} factor that interacts with FliA_{Td} and prevents it from binding to the σ^{28} -dependent promoter.

FlgM_{Td} controls *T. denticola* flagellar filament gene expression. To investigate the role of FlgM_{Td} in *T. denticola*, we constructed an *flgM*_{Td} deletion mutant (Δ *flgM*) and its isogenic complemented strain (*cfgM*) using a strategy illustrated in Fig. S1 in the supplemental material. Immunoblotting assays with anti-FlgM_{Td} showed that the production of FlgM_{Td} was abolished in the Δ *flgM* mutant and then restored in the *cfgM* strain (Fig. 6A). Deletions of *flgM* genes typically increased class 3 flagellar gene expression (16, 23). Unexpectedly, our im-

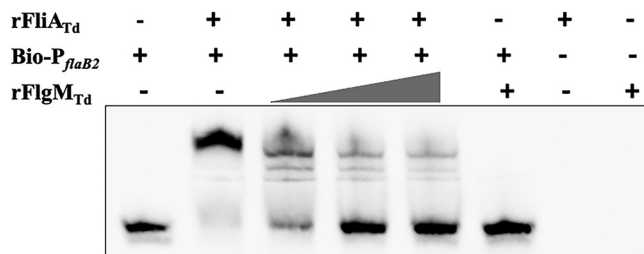


FIG 5 FlgM_{Td} sequesters FliA_{Td} from binding to the *flaB2* promoter. EMSA was performed using biotin-labeled *flaB2* promoter (Bio- P_{flaB2}) as a DNA probe. For this assay, Bio- P_{flaB2} was incubated with a fixed amount of recombinant FliA_{Td} protein (rFliA_{Td}) and then titrated with increasing concentrations of recombinant FlgM_{Td} protein (rFlgM_{Td}) as labeled.

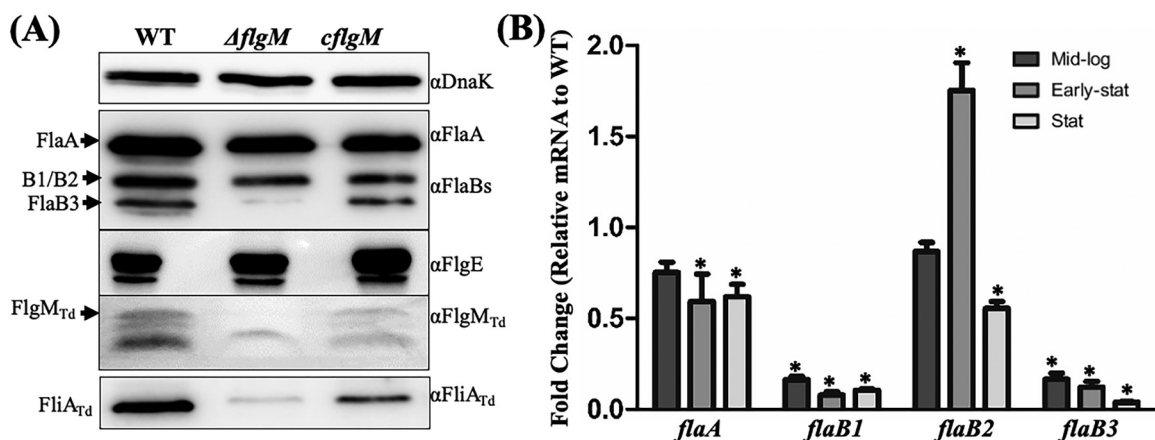


FIG 6 Deletion of *flgM_{Td}* impairs *T. denticola* flagellar filament gene expression. (A) Immunoblotting analysis. Equivalent amounts of whole-cell lysates of the wild-type (WT), $\Delta flgM$, and *cflgM* strains were analyzed by SDS-PAGE and then probed with specific antibodies against the following proteins: DnaK (loading control), FlaA, FlaBs, FlgE, FlgM_{Td}, and FliA_{Td}. (B) qRT-PCR analysis. For this experiment, the levels of four flagellar filament genes (*flaA*, *flaB1*, *flaB2*, and *flaB3*) were measured by qRT-PCR as previously described (41, 48). The *dnaK* gene transcript was used as an internal control to normalize the readouts of qRT-PCR. The results are expressed as the level of individual gene transcripts in the $\Delta flgM$ mutant relative to that of the wild type at three different growth phases, including the mid-logarithmic (Mid-log), early stationary (Early-stat), and stationary (Stat) phases. Asterisks indicate that the difference between the wild-type and $\Delta flgM$ strains was statistically significant at a P value of <0.01 (one-way ANOVA followed by Tukey's multiple-comparison test).

munoblotting results uncovered that deletion of *flgM_{Td}* significantly reduced the level of four flagellar filament proteins in *T. denticola*, including FlaA, FlaB1, FlaB2, and FlaB3, whereas the level of the hook protein FlgE remained unchanged (Fig. 6A). The result from FlgE is expected because it belongs to the class 2 flagellar genes, which are regulated by σ^{70} in the flagellar transcriptional cascade of *E. coli* and *S. Typhimurium* (2, 55). To elucidate the mechanism underpinning the reduction of four flagellar filament proteins in the $\Delta flgM$ mutant, we monitored their transcript (mRNA) levels during growth by using quantitative RT-PCR (qRT-PCR) and found that the expression of *flaA*, *flaB1*, and *flaB3* genes was constantly impaired in the $\Delta flgM$ mutant at the mid-log, early stationary, and stationary phases (Fig. 6B). Compared to the wild type, expression of the *flaB2* gene in the $\Delta flgM$ mutant was more diverse (Fig. 6B), ranging from a slight reduction at log phase, transient increase at early stationary phase, and $\sim 50\%$ reduction at stationary phase. We repeated this experiment three times with different biological samples and found a similar pattern. This result indicates that the reduction of four flagellar filament proteins in the $\Delta flgM$ mutant mainly occurs at the transcriptional level.

Our recent reports show that the *flaB2* gene is positively regulated by FliA_{Td} (41, 48). Thus, we expected that deletion of FlgM_{Td}, an anti- σ^{28} factor, should increase its expression. Along with this expectation, we found that the level of *flaB2* mRNA was transiently elevated at the early stationary phase of the $\Delta flgM$ mutant. However, its expression level was attenuated at the stationary phase, which is contradictory to the role of FlgM_{Td} as an anti- σ^{28} factor. To explore its underlying mechanism, we first measured the level of FliA_{Td} by immunoblotting with anti-FliA_{Td} and found that its level significantly decreased in the mutant (Fig. 6A). FlgM interacts with FliA, forming a complex in the cytoplasm (50). We reasoned that deletion of FlgM_{Td} may affect the stability of FliA_{Td}, which in turn impairs flagellin gene expression in the mutant. To test this possibility, we carried out protein turnover assays to monitor the stability of FliA_{Td}. Our results uncovered that while FliA_{Td} was stable in wild type during the course of 24 h, it was rapidly degraded in the $\Delta flgM$ mutant: e.g., 6 h after arresting protein synthesis with spectinomycin, FliA_{Td} was almost undetectable (Fig. 7A). This result can explain the reduction of *flaB2* mRNA, a gene regulated by FliA_{Td} (σ^{28}). It is possible that without FlgM_{Td}, free FliA_{Td} in the cytoplasm is degraded by certain proteases that are activated when *T. denticola* enters the stationary phase, which in turn impairs the expression of the *flaB2* gene. Supporting this possibility, a similar scenario is reported in *E. coli*, whereby FlgM protects FliA from proteolysis, which mainly depends on the Lon protease (56).

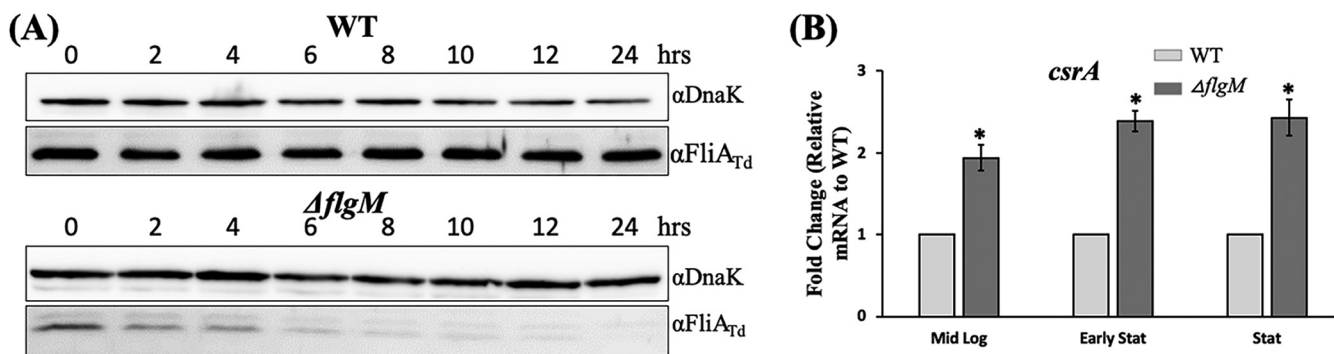


FIG 7 Deletion of *flgM_{Td}* leads to FliA_{Td} degradation and increases expression of the *csrA* gene. (A) Protein turnover assays of the wild type (WT) and the $\Delta flgM$ mutant. Protein translation was arrested by adding spectinomycin to the mid-log cultures. Samples were collected at the indicated time points and analyzed by immunoblotting. Equivalent amounts of whole-cell lysates were analyzed by SDS-PAGE and then probed with specific antibodies to DnaK ($\alpha DnaK$) and FliA_{Td} ($\alpha FliA_{Td}$), and DnaK was used as a loading control. (B) Detection of *csrA* (*TDE2355*) gene transcripts using qRT-PCR. Similar to the above qRT-PCR analysis, *dnaK* was used as an internal control to normalize the readouts of qRT-PCR, and the results are expressed as the level of individual gene transcripts in the $\Delta flgM$ mutant relative to those of the wild type at the mid-log, early stationary, and stationary phases. Asterisks indicate that the difference between the wild-type and $\Delta flgM$ strains was statistically significant at a P value of <0.01 .

It was unexpected that deletion of *flgM_{Td}* led to the reduction of *flaA*, *flaB1*, and *flaB3* transcripts (Fig. 6) because they are regulated by σ^{70} rather than σ^{28} (41, 57). CsrA (carbon storage regulator A) is a small RNA binding protein that represses flagellin gene expression in several bacteria both transcriptionally and translationally (32, 58, 59). CsrA is also a global regulator that orchestrates vast gene expression, including σ factors such as FliA (60). The genome of *T. denticola* encodes a CsrA homolog (*TDE2355*) (61), and its binding site is found at the upstream untranslated regions (UTRs) of the *flaA*, *flaB1*, and *flaB3* genes (data not shown); thus, we speculated that deletion of *flgM_{Td}* may increase expression of *TDE2355* which, in turn, represses expression of the *flaA*, *flaB1*, and *flaB3* genes. To determine if this possibility stands, we measured the *TDE2355* mRNA using qRT-PCR and found that its level was significantly increased in the mutant at the log, early stationary, and stationary phases (Fig. 7B), which coincides with the reduction of *flaA*, *flaB1*, and *flaB3* mRNA. A similar phenotype is also reported in *Yersinia pseudotuberculosis* (62). Taken together, these results indicate that while FliA_{Td} is an anti- σ^{28} factor, its role and mechanism of action are more complex than those of its counterparts in other bacteria. This unique regulatory mechanism may allow the spirochete to finely govern the level of multiple flagellin proteins to assemble flagellar filaments, which are structurally more complex than most external flagellates.

FliA_{Td} is essential for the motility of *T. denticola*. Deletion of *flgM_{Td}* has no impact on *T. denticola* growth because the growth rate of the $\Delta flgM$ mutant was similar to those of the wild-type and *cflgM* strains (Fig. 8A). Under dark-field microscopy, we found that the $\Delta flgM$ mutant swam poorly and was unable to displace in 1% methylcellulose (Videos S1 to S3), suggesting that its motility was impaired. To confirm this observation, we carried out swimming plate assays (Fig. 8B) and found that the swimming rings of the $\Delta flgM$ mutant (5.25 ± 0.17 mm; $n = 16$ plates) were significantly smaller than those of the wild type (18.75 ± 0.24 mm; $n = 16$ plates) and the complemented strain (11.62 ± 0.38 mm; $n = 16$ plates) (Fig. 8C). This result was further confirmed by bacterial motion tracking analysis, wherein individual bacterial cells were tracked for at least 30 s in 1% methylcellulose, and their average velocities ($\mu\text{m/s}$, $n = 26$ cells) were measured as follows: wild type, 10.31 ± 0.6 $\mu\text{m/s}$; $\Delta flgM$ strain, 1.39 ± 0.23 $\mu\text{m/s}$; and *cflgM* strain, 6.82 ± 0.39 $\mu\text{m/s}$. These results indicate that FliA_{Td} is indispensable for *T. denticola* motility, in contrast to its counterparts in other bacteria, where deletions of *flgM* genes either have no significant impact on motility or lead to abnormal swimming behaviors (16, 23, 63, 64). We noticed that the motility of *cflgM* was not fully restored. This may be because the expression level or timing of *flgM_{Td}* in the complemented strain does not fully coincide with that of wild type. This strain was created by *cis*-complementation. We also tried to complement the $\Delta flgM$ mutant using pBFC, a shuttle vector of *T. denticola* (65, 66); however, this vector is poorly transformable in the parental wild-type ATCC 35405 strain (65).

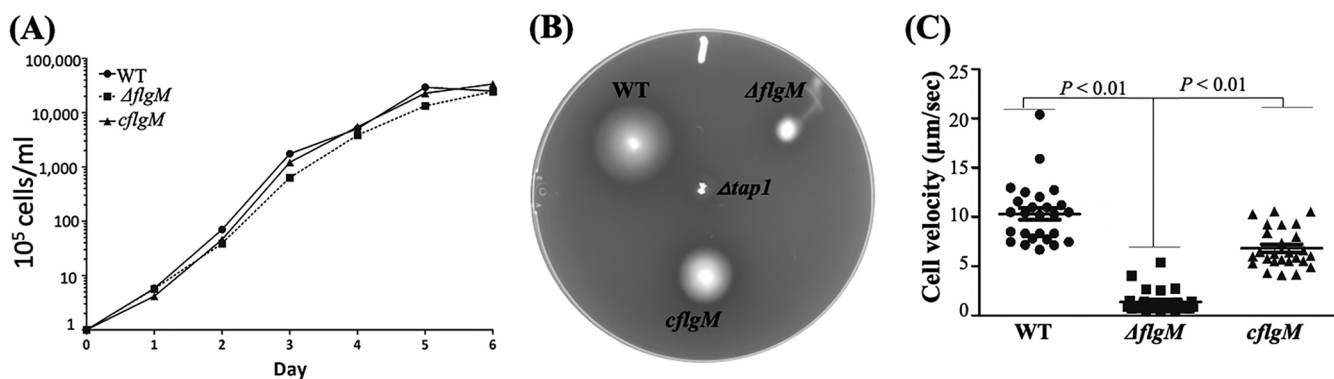


FIG 8 Deletion of *flgM_{7d}* has no impact on *T. denticola* growth but inhibits its motility. (A) Growth curves of the wild-type (WT), $\Delta flgM$, and *cflgM* strains. For this experiment, 10^5 *T. denticola* cells were inoculated into the TYGVS medium and enumerated every 24 h for up to 6 days using a Petroff-Hausser counting chamber. (B) Swimming plate assays. This assay was carried out on 0.35% agarose containing the TYGVS medium diluted 1:1 with PBS. The plates were incubated anaerobically at 37°C for 3 days. The $\Delta tap1$ strain, a nonmotile mutant, was used as a control to determine initial inoculum sizes. (C) Cell tracking analysis of the wild-type, $\Delta flgM$, and *cflgM* strains. *T. denticola* cells were tracked in the presence of 1% methylcellulose as previously described (57). The results are expressed as average cell velocities (micrometers per second) of at least 20 cells. The data were analyzed by one-way ANOVA, followed by Tukey's multiple-comparison test at $P < 0.01$.

Deletion of *flgM_{7d}* alters the flagellar polarity of *T. denticola*. To determine if deletion of *flgM_{7d}* impairs *T. denticola* flagellar assembly, we applied cryo-ET to directly visualize PFs inside the cells. In total, we generated 20 whole-cell reconstructions, including wild-type (3 cells), $\Delta flgM$ (10 cells), and *cflgM* (7 cells) strains. We also enumerated the number of flagellar motors and measured the length of PFs (Table 1). As in our previous reports (41, 42, 48, 57), *T. denticola* wild-type cells uniformly have bipolar flagella (two PFs at both cell poles), which form two helical bundles wrapping around

TABLE 1 Cryo-ET analysis of the wild type, $\Delta flgM$, and *cflgM* strains

| Strains | No. of motors | PF length(s) (μm) in ^a : | |
|--|---------------|--|----------------------------|
| | | New pole | Old pole |
| Wild type | | | |
| Cell 1 | 4 | 2.1 and 2.1 | 4.8 and 6.1 |
| Cell 2 | 4 | 3.5 and 2.5 | 5.0 and 5.5 |
| Cell 3 | 4 | 3.4 and 3.5 | 4.6 and 4.6 |
| Avg | 4 | 2.9 ± 0.7 ($n = 6$) | 5.1 ± 0.6 ($n = 6$) |
| $\Delta flgM$ mutant | | | |
| Cell 1 | 3 | 2.5 | 5.0 |
| Cell 2 | 4 | ND | ND |
| Cell 3 | 3 | ND | 5.5 and 5.5 |
| Cell 4 | 4 | ND | 6.0 and 6.0 |
| Cell 5 | 3 | ND | 6.5 and 6.5 |
| Cell 6 | 3 | ND | 4.0 and 4.5 |
| Cell 7 | 3 | ND | 4.0 and 6.0 |
| Cell 8 | 3 | ND | 5.8 and 6.0 |
| Cell 9 | 3 | ND | 4.0 and 6.0 |
| Cell 10 | 4 | ND | 5.0 and 6.0 |
| Avg | 3.3 | ND | 5.6 ± 0.7 ($n = 17$) |
| <i>cflgM</i> complemented clone | | | |
| Cell 1 | 4 | 4.0 and 4.0 | 5.0 and 5.0 |
| Cell 2 | 4 | 3.0 and 4.5 | 5.0 and 5.0 |
| Cell 3 | 4 | 4.5 and 5.0 | 5.0 and 5.0 |
| Cell 4 | 4 | 1.5 and 1.5 | 6.0 and 6.0 |
| Cell 5 | 4 | 0.5 and 1.5 | 5.5 and 5.5 |
| Cell 6 | 4 | 3.0 and 6.5 | 6.5 and 6.5 |
| Cell 7 | 4 | 6.5 and 5.0 | 6.5 and 6.0 |
| Avg | 4 | 3.6 ± 1.9 ($n = 14$) | 5.6 ± 0.7 ($n = 14$) |

^aND, no PFs detected; n , number of PFs.

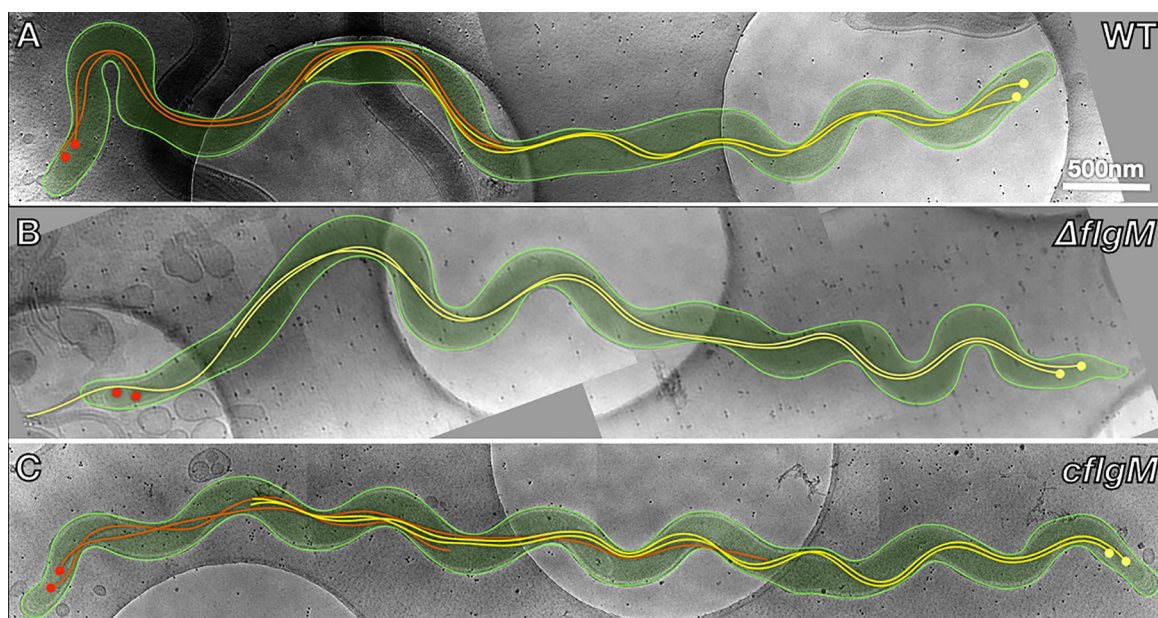


FIG 9 Whole-cell cryo-ET analysis of the wild-type, $\Delta flgM$, and $cflgM$ cells. Shown are projection images of a wild-type cell (A), $\Delta flgM$ cell (B), and $cflgM$ cell (C). PFs originating from one end of cells are colored in yellow and those from the opposite end in orange.

the cell cylinders (Fig. 9A). Interestingly, the two bundles of PFs are asymmetrical in terms of length (i.e., the PFs from one end of the cells are usually longer than those from the opposite end). Jutras et al. uncovered that *T. denticola* forms a single division zone and divides near the middle of the cells (67); thus, a nascent daughter cell might inherit one bundle of PFs from the old cell pole and newly assemble the other bundle of PFs at the new cell pole. Therefore, we referred to the pole with long PFs as the “old pole” and the one with short PFs as the “new pole.” We measured the lengths of PFs and found that those from “old pole” ($5.0 \pm 0.6 \mu\text{m}$; $n = 6$ PFs) are nearly two times longer than those from “new pole” ($2.9 \pm 0.7 \mu\text{m}$; $n = 6$ PFs). A similar phenotype was also observed in the complemented strain (Table 1). The phenotype of the $\Delta flgM$ mutant is quite striking. Instead of having bipolar PFs, as observed in both the wild-type and $cflgM$ strains, the majority of mutant cells (8/10) had two PFs at only one end of cells (Fig. 9B and Table 1). Of the remaining two mutant cells, one had a single flagellum at each cell end, and the other had no PFs. We found that the number of flagellar motors (3.3 motors per cell) in the mutant is slightly lower than that of wild type (4 motors per cell) but not statistically significant (Table 1). We also measured the length of PFs *in situ* and found that the remaining two PFs in the mutant ($5.2 \pm 1.1 \mu\text{m}$; $n = 18$ PFs) are longer ($P < 0.05$) than those in the wild type ($3.9 \pm 1.3 \mu\text{m}$; $n = 12$ PFs). Occasionally, those PFs were too long and even protruded from the cells (Fig. 9B). These results indicate that deletion of $flgM_{Td}$ has limited impact on the number of flagellar motors but does alter the flagellar filament number, length, and polarity in *T. denticola*. To our knowledge, a similar phenotype has not been reported in other bacteria.

Summary. The above studies provide several lines of evidence that TDE0201 is a FlgM homolog: (i) it has a structural topology similar to that of its counterparts from other bacteria (Fig. 1), (ii) it represses *E. coli* motility and *flhC* expression (Fig. 2), and (iii) it interacts with the *T. denticola* σ^{28} (FliA_{Td}) and prevents it from binding to the σ^{28} -dependent promoters (Fig. 4 and 5). Identification of FlgM_{Td} and FliA_{Td} indicates that *T. denticola* has also evolved to regulate its later flagellar gene expression through the partner-switching mechanism between σ^{28} and its antagonist FlgM. We also searched the genomes of other spirochetes using FliA_{Td} and FlgM_{Td} as queries and identified their homologs in *T. pallidum*, *Brachyspira*, and *Leptospira* species: e.g., FliA_{Td} and FlgM_{Td} share 69% and 39% sequence identities with TP_0709 and TP_0974 of *T.*

pallidum (68), respectively, suggesting that a similar regulatory mechanism also exists in other spirochetes. Therefore, the results presented in this report also shed light on the role of FliA and FlgM homologs in other spirochetes. Our results also demonstrate that FlgM_{Td} acts differently from its counterparts in other bacteria in several ways: (i) FlgM_{Td} protects FliA_{Td} from being degraded (e.g., deletion of *flgM_{Td}* leads to FliA_{Td} rapid turnover) (Fig. 7), (ii) deletion of *flgM_{Td}* represses flagellin gene expression in *T. denticola* (Fig. 6), rather than increasing flagellin gene expression as reported in other bacteria, (iii) FlgM_{Td} interplays with other regulators, such as CsrA (Fig. 7), and (iv) deletion of *flgM_{Td}* alters the flagellar polarity from bipolar to monopolar (Fig. 9). We found that the reduction of flagellin gene expression in the Δ *flgM* mutant is mainly due to FliA_{Td} turnover and CsrA upregulation. However, the mechanism by which FlgM_{Td} regulates flagellar polarity remains unknown. Previous studies have shown that small GTPase FlhF and FlhG act cooperatively to harness flagellar number and placement in several polar flagellates, such as *B. burgdorferi* (31), *C. jejuni* (69), and *Vibrio alginolyticus* (70). Additionally, FapA (flagellar assembly protein A) controls the flagellar polarity of *Vibrio vulnificus* (71, 72). We recently found FlhF (TDE2686), FlhG (TDE2685), and FapA (TDE2682) homologs in a large motility gene operon of *T. denticola* (48). Therefore, it is possible that FlgM_{Td} regulates flagellar polarity by directly or indirectly modulating these proteins. We are planning to perform chromatin immunoprecipitation sequencing (ChIP-seq) to map the promoters recognized by FliA_{Td} and transcriptome sequencing (RNA-seq) to determine genes coordinately regulated by FliA_{Td} and FlgM_{Td}. Results from these studies will provide insights into the role that FlgM_{Td} plays in control of *T. denticola* flagellar polarity.

MATERIALS AND METHODS

Bacterial strains, culture conditions, and oligonucleotide primers. *Treponema denticola* ATCC 35405 (wild type [WT]) was used in this study (61). Cells were grown in tryptone-yeast extract-gelatin-volatile fatty acids-serum (TYGVS) medium at 37°C in an anaerobic chamber in the presence of 85% nitrogen, 5% carbon dioxide, and 5% hydrogen (73). *T. denticola* isogenic mutants were grown with appropriate antibiotic for selective pressure as needed: erythromycin (50 μ g/mL) and gentamicin (20 μ g/mL). The *Escherichia coli* DH5 α strain (New England Biolabs, Ipswich, MA) was used for DNA cloning. BL21 Star(DE3) (Invitrogen, Waltham, MA) was used for preparing recombinant proteins. The *E. coli* strains were cultivated in lysogeny broth (LB) supplemented with appropriate concentrations of antibiotics for selective pressure as needed: erythromycin, 400 μ g/mL; gentamicin, 20 μ g/mL; kanamycin 50 μ g/mL; and ampicillin, 100 μ g/mL. The oligonucleotide primers for PCR and RT-PCR used in this study are listed in Table S1 in the supplemental material. These primers were synthesized in Integrated DNA Technologies (IDT, Coralville, IA).

Electrophoresis and immunoblotting analysis. Sodium dodecyl sulfate-polyacrylamide gel electrophoresis (SDS-PAGE) and immunoblotting analyses were carried out as previously described (48). For immunoblotting, *T. denticola* cells were harvested in the mid-logarithmic (mid-log) phase ($\sim 5 \times 10^8$ cells/mL). Equal amounts of whole-cell lysates (1 to 5 μ g) were separated by SDS-PAGE and then transferred to polyvinylidene difluoride (PVDF) membranes. The immunoblots were probed with specific antibodies against *T. pallidum* FlaB and *T. denticola* FlaA, DnaK, FlgE, and FliA as described in previous publications (48, 74, 75). The antibody against *T. denticola* TDE0201 was generated in rats in this study (see below for details). His tag and FLAG tag antibodies were purchased from Thermo Fisher Scientific (Waltham, MA) and Sigma-Aldrich (St. Louis, MO). *E. coli* flagellin (FlhC) and GroEL antibodies were purchased from Abcam (Cambridge, United Kingdom). Immunoblots were developed using a horseradish peroxidase-conjugated secondary antibody with an enhanced chemiluminescence (ECL) assay, and signals were quantified using the Molecular Imager ChemiDoc system with the Image Lab software (Bio-Rad Laboratories, Hercules, CA) as previously described (57).

Preparation of TDE0201 recombinant protein and its antiserum. The gene encoding the full-length TDE0201 protein was PCR amplified with primers P₁/P₂ using Pfx DNA polymerase (Life Technologies, Grand Island, NY) and then cloned into the pET200/d-TOPO expression vector (Life Technologies), which encodes a 6-histidine-tag (6 \times His) at the N terminus. The resulting plasmids were then transformed into BL21 Star(DE3) (Invitrogen). The expression of TDE0201 was induced using 1 mM isopropyl- β -D-1-thiogalactopyranoside (IPTG). For antiserum preparation, the recombinant TDE0201 protein was purified using Ni-nitrilotriacetic acid (NTA) agarose (Qiagen, Valencia, CA) under denaturing conditions according to the manufacturer's protocol (Qiagen). For the electrophoretic mobility shift assay (EMSA), the recombinant proteins were purified using Ni-NTA agarose (Qiagen) under native conditions in the presence of 1% Sarkosyl according to the manufacturer's protocol (Qiagen). The purified proteins were then dialyzed in 20 mM Tris-HCl buffer (pH 8.0) at 4°C overnight using 3.0-kDa molecular-weight-cutoff Spectra/Por dialysis bags (Spectrum Laboratories, Rancho Dominguez, CA). The concentrations of purified proteins were determined using a Bio-Rad Protein assay kit (Bio-Rad). The antibody against TDE0201 was produced by General Bioscience (Brisbane, CA) as previously described (48). In brief, 5 mg of purified recombinant TDE0201 was used to immunize two rats following a standard immunization procedure. The primers for preparation of the recombinant proteins are listed in Table S1.

Heterologous expression of TDE0201 in *E. coli*. The gene encoding the full-length TDE0201 protein was PCR amplified with primers P₄₀/P_{41r}, and the resulting amplicon was first cloned into pGEM-T Easy vector (Promega, Madison, WI) and then subcloned into pFLAG-CTS expression vector (Sigma-Aldrich). The resulting plasmid (pFLAG-CTS-TDE0201) and pFLAG-CTS (negative control) were transformed into the *E. coli* DH5 α strain, respectively. The resulting DH5 α strains were subjected to immunoblotting analysis with FLAG antibody (anti-Flag) for detection of TDE0201 and anti-FliC for detection of *E. coli* FliC expression, as well as to swimming plate assays for assessing the impact of TDE0201 on *E. coli* motility. Swimming plate assays of *E. coli* were performed on soft agar plates containing 1% tryptone, 0.5% NaCl, and 0.3% agar as previously described (48). In brief, overnight *E. coli* cultures were diluted to 1:100. After 8 h of growth at 37°C, 1 μ L of the culture was inoculated onto the soft agar plates with or without IPTG (1 mM), and then the plates were incubated at 30°C for 16 h. The average diameters of swimming rings were calculated from four independent plates; the results are represented as the mean of diameters \pm standard error of the mean (SEM). The data were statistically analyzed by one-way analysis of variance (ANOVA), followed by Tukey's multiple-comparison test at $P < 0.01$.

Construction of a TDE0201 deletion mutant and its complemented strain. The TDE0201::erm (Fig. S1A) plasmid was constructed to replace the entire open reading frame of TDE0201 with a previously documented erythromycin resistance cassette (*ERM-F/AM*) (76). The vector TDE0201^{com} (Fig. S1B) was constructed to *cis*-complement the TDE0201 deletion mutant. These two plasmids were constructed by two-step PCR and DNA cloning. To construct TDE0201::erm, the TDE0201 upstream region, *ERM-F/AM*, and the TDE0201 downstream region were PCR amplified with primers P₃/P_{4r}, P₅/P_{6r}, and P₇/P_{8r}, respectively. The resulting PCR fragments were cloned into the pGEM-T Easy vector (Promega, Madison, WI). The upstream and downstream regions were ligated. The resulted fragment was then inserted by *ERM-F/AM* at an engineered XbaI cut site, generating TDE0201::erm, as illustrated in Fig. S1A. To delete TDE0201, TDE0201::erm was linearized and transformed into *T. denticola* wild-type competent cells via heat shock as previously described (77). The deletion was confirmed by PCR and immunoblotting analyses. The resulting mutant was designated the Δ flgM strain. To construct TDE0201^{com}, the full-length TDE0201 gene along with its upstream region and the *aacC1* cassette were PCR amplified with primers P₃/P₉ and P₁₀/P_{11r}, respectively, and then fused together with primers P₃/P_{11r}, generating TDE0201-*aacC1*. The downstream region of TDE0201 was PCR amplified with primers P₁₂/P₈ and then fused to TDE0201-*aacC1* by PCR using primers P₃/P₈ (Fig. S1B). The obtained DNA fragment was cloned into the pGEM-T Easy vector, generating the vector TDE0201^{com}. To restore the expression of TDE0201, TDE0201^{com} was linearized and transformed into the Δ flgM mutant via heat shock (77). The resulting complemented clones were confirmed by PCR and immunoblotting analyses. One complemented clone (*flgM*) was selected for further characterizations. The primers for constructing these two plasmids are listed in Table S1.

Coimmunoprecipitation. Coimmunoprecipitation (co-IP) was carried out as previously described (57). Briefly, 500 mL of the mid-log-phase *T. denticola* wild-type and Δ flgM mutant (negative control) cultures ($\sim 5 \times 10^8$ cells/mL) was centrifuged at $5,000 \times g$ for 20 min at 4°C. The obtained cell pellets were washed three times with phosphate-buffered saline (PBS [pH 7.4]) and then resuspended in 2 mL of TSEA buffer (50 mM Tris-HCl, 150 mM NaCl, 5 mM EDTA, 0.05% sodium azide [pH 7.5]). The resulting cell suspensions were sonicated on ice, followed by centrifugation ($14,800 \times g$ for 30 min at 4°C) to collect the cell supernatants. For co-IP, $\sim 500 \mu$ L supernatant was incubated with 100 μ L of FliA_{Td} antibody (anti-FliA_{Td}) for 16 h at 4°C in the presence of 1% bovine serum albumin (BSA). After the incubation, $\sim 50 \mu$ L of protein A agarose (Sigma-Aldrich) was added, and the mixture was further incubated for 16 h at 4°C. The resulting samples were centrifuged ($1,600 \times g$ at 4°C) and then washed three times with 1 mL of PBS buffer containing 0.05% Tween 20. The final pellets were suspended in 50 μ L of electrophoresis sample buffer, boiled for 5 min, and then briefly centrifuged as before to collect the supernatants, which were then subjected to SDS-PAGE and immunoblotting analysis.

Coexpression of recombinant TDE2683 (FliA_{Td}) and TDE0201 (FlgM_{Td}) proteins. To determine if FlgM_{Td} binds to FliA_{Td}, these two proteins were coexpressed in *E. coli* with either a His tag (His-FliA_{Td}) or a FLAG tag (FlgM_{Td}-FLAG) as previously described (58, 78). Briefly, the genes encoding the full-length FliA_{Td} and FlgM_{Td} were amplified with primers P₁₃/P₁₄ and P₁₅/P_{16r}, respectively, and then fused together with primers P₁₃/P₁₆. Of note, the sequence encoding FLAG was added to the 3' end of TDE0201 and a stop codon was added between these two genes. The resulting amplicons were cloned into pGEM-T Easy vector (Promega) and then subcloned into pQE80L expression vector (Qiagen), which encodes the 6 \times His tag at the N terminus. The resulting plasmids were transformed into BL21 Star(DE3) (Invitrogen). Recombinant His-FliA_{Td} and FlgM_{Td}-FLAG proteins were induced using 1 mM isopropyl β -D-1-thiogalactosidase (IPTG) and then purified using either Ni-NTA agarose (Qiagen) or anti-Flag M2 affinity gel (Sigma-Aldrich) under native conditions according to the manufacturers' protocols.

Bacterial swimming plate assay and motion tracking analysis. Swimming plate assays were performed as previously described (41). Briefly, 4 μ L of *T. denticola* cultures (10^9 cells/mL) was inoculated onto 0.35% agarose containing TYGV5 medium diluted 1:1 with PBS. The plates were incubated anaerobically at 37°C for 3 days to allow the cells to swim out. The diameters of swimming rings were measured in millimeters. As a negative control, a previously constructed nonmotile mutant of *T. denticola* (Δ tap1) was included to determine the initial inoculum size (79). The average diameters of each strain were calculated from at least four independent plates; the results are represented as the mean of diameters \pm standard error of the mean (SEM). The velocity of bacterial cells was measured using a computer-based bacterial tracking system as previously described (57). Briefly, 100 μ L of mid-log-phase *T. denticola* cultures was first diluted (1:50) in oral bacterial growth medium (OBGM), and then 10 μ L of diluted cultures was mixed with an equal volume of 2% methylcellulose with a viscosity of 4,000 cp (80). *T.*

denticola cells were videotaped and tracked. For each bacterial strain, 26 cells were recorded for up to 30 s. The average cell swimming velocities (micrometers per second) of tracked cells were calculated.

Measuring *T. denticola* growth rates. For this study, a total of 10^5 cells/mL of late-log-phase *T. denticola* cultures was inoculated into 5 mL TYGVS medium and then were enumerated every 24 h using a Petroff-Hausser counting chamber (Hausser Scientific, Horsham, PA). Each growth curve is representative of at least three independent cultures, and the results are represented as the mean of cell numbers \pm standard error of mean (SEM).

Measuring the level of FlgM_{Td} throughout the growth phase of *T. denticola*. For this study, the wild-type strain and a previously constructed *flgE*-deficient mutant ($\Delta flgE$) of *T. denticola* were used (61, 76). A total of 2×10^6 cells/mL of late-log-phase *T. denticola* cultures was inoculated into the TYGVS medium. *T. denticola* cells in the cultures were enumerated every 24 h using a Petroff-Hausser counting chamber (Hausser Scientific, Horsham, PA). Samples were harvested at different time points and subjected to immunoblotting analysis.

RNA preparations, qRT-PCR, and 5'-RACE. RNA isolations were performed as previously described (42). Briefly, a total of 10^5 cells/mL of late-log-phase *T. denticola* cultures was inoculated into 100 mL TYGVS medium. *T. denticola* cells in the cultures were enumerated every 24 h using a Petroff-Hausser counting chamber (Hausser Scientific). Samples were harvested at different time points. Total RNA was extracted using TRI reagent (Sigma-Aldrich), following the manufacturer's instructions. The resulting samples were treated with Turbo DNase I (Thermo Fisher Scientific) at 37°C for 2 h to eliminate genomic DNA contamination. The resulting RNA samples were reextracted using acid phenol-chloroform (Ambion), precipitated in isopropanol, and washed once with 70% ethanol. The RNA pellets were resuspended in RNase-free water. cDNA was generated from the purified RNA (1 μ g) using a SuperScript IV VIL0 cDNA synthesis kit (Thermo Fisher Scientific). qRT-PCR was performed using iQ SYBR green supermix and an MyiQ thermal cycler (Bio-Rad). The gene encoding DnaK (*TDE0628*) was used as an internal control to normalize the qRT-PCR data as previously described (42). The results were expressed as the normalized difference of threshold cycles ($\Delta\Delta C_T$) between the wild type and $\Delta flgM$ mutant. 5'-RACE analysis was performed using the SMART RACE 5'/3' kit (TaKaRa Bio USA) according to the manufacturer's protocol. The primers for RT-PCR, qRT-PCR, and 5'-RACE are listed in Table S1.

Protein turnover assay. The protein turnover assay was carried out as previously described (42, 57). Briefly, *T. denticola* strains were first grown to the mid-log phase ($\sim 5 \times 10^8$ cells/mL). Subsequently, spectinomycin (100 μ g/mL) was added into the cultures, followed by incubation at 37°C. Samples (10 mL) were harvested at the indicated time points and subjected to immunoblotting analysis.

EMSA. The electrophoretic mobility shift assay (EMSA) was performed using recombinant proteins FliA_{Td} (rFliA_{Td}) and FlgM_{Td} (rFlgM_{Td}), as well as the *flaB2* promoter (P_{flaB2}) as a DNA probe, as previously described (48). The DNA probe was synthesized by PCR using primers P₁₇/P₁₈ (Table S1) and labeled with biotin using the Biotin DecaLabel DNA labeling kit (Thermo Fisher Scientific). EMSA was performed by adding increasing amounts of rFlgM_{Td} (25.8 μ M, 65 μ M, and 130 μ M) to biotin-labeled P_{flaB2} (2 mM) in binding buffer (10 mM Tris-HCl [pH 7.5]). The mixtures were incubated at room temperature for 30 min. After the incubation, 25.8 μ M rFliA_{Td} was added to the reaction mixtures and the mixtures were further incubated for another 1 h. DNA loading dye was then added to the reaction mixtures immediately before loading. The reaction mixtures were separated on 4 to 20% Mini-Protean TGX gels using 0.5 \times Tris Borate EDTA (TBE) buffer and then transferred to a nylon membrane and cross-linked using UV light. The detection was performed using a Chemiluminescent nucleic acid detection module kit (Thermo Fisher Scientific).

Cryo-ET sample preparation, data collection, and image processing. The freeze-hydrated specimens of *T. denticola* were prepared as previously described (42). Briefly, *T. denticola* cultures were mixed with 10-nm colloidal gold solutions and then deposited on a freshly glow-discharged, holey carbon grid for about 1 min. The grids were blotted with a small piece of filter paper for ~ 4 s and then rapidly plunged into liquid ethane using a gravity-driven plunger apparatus. The grids were then transferred to a 300-kV Krios electron microscope (Thermo Fisher Scientific) equipped with a field emission gun, Volta phase plate (VPP), and a direct detection detector (Gatan). To generate three-dimensional (3D) reconstructions of whole bacterial cells, SerialEM (81) was used to acquire multiple tilt series along the cell at a $\times 19,000$ magnification. The pixel size at the specimen level is 5.4 Å. Tilt series were collected in the low-dose mode with the VPP at an ~ 0.5 - μ m defocus. A total dose of 60 e⁻/Å² was distributed among 33 tilt images covering angles from -48° to $+48^\circ$ at tilt steps of 3°. The tilt series were aligned and reconstructed by IMOD (82). Multiple reconstructions from different segments of the same cell were integrated into one large reconstruction. In total, we generated over 90 tomograms to build 20 reconstructions of the entire cells from the wild-type (3 cells), $\Delta flgM$ (10 cells), and *flgM* (7 cells) strains.

Bioinformatics and statistical analyses. Sequence alignment analyses were performed using Clustal Omega. Homology modeling was generated using MODELLER version 10.0 (83), as incorporated in the MPI Bioinformatics Toolkit (84), and protein-protein docking analysis was conducted using the ClusPro server (85). Statistical significance was analyzed by one way ANOVA followed by Tukey's multiple-comparison test at $P < 0.01$.

SUPPLEMENTAL MATERIAL

Supplemental material is available online only.

SUPPLEMENTAL FILE 1, PDF file, 0.5 MB.

SUPPLEMENTAL FILE 2, MPG file, 0.9 MB.

SUPPLEMENTAL FILE 3, MPG file, 0.9 MB.

SUPPLEMENTAL FILE 4, MPG file, 0.9 MB.

ACKNOWLEDGMENTS

This research was supported by funding from the National Institute of Dental and Craniofacial Research (DE023080 to C. Li) and National Institutes of Allergy and Infectious Diseases (AI078958 to C. Li, AI087946 to J. Liu, and AI148844 to Brian Crane and C. Li), National Institutes of Health (NIH). Cryo-ET data were collected at Yale Electron Cryo-Microscopy Resources, which is funded in part by NIH grant 1S10OD023603-01A1.

We thank Jennifer Aronson for critical reading of the manuscript.

REFERENCES

- Erhardt M, Namba K, Hughes KT. 2010. Bacterial nanomachines: the flagellum and type III injectisome. *Cold Spring Harb Perspect Biol* 2:a000299. <https://doi.org/10.1101/cshperspect.a000299>.
- Cheavance FF, Hughes KT. 2008. Coordinating assembly of a bacterial macromolecular machine. *Nat Rev Microbiol* 6:455–465. <https://doi.org/10.1038/nrmicro1887>.
- Armitage JP, Berry RM. 2020. Assembly and dynamics of the bacterial flagellum. *Annu Rev Microbiol* 74:181–200. <https://doi.org/10.1146/annurev-micro-090816-093411>.
- Meister M, Berg HC. 1987. The stall torque of the bacterial flagellar motor. *Biophys J* 52:413–419. [https://doi.org/10.1016/S0006-3495\(87\)83230-7](https://doi.org/10.1016/S0006-3495(87)83230-7).
- Meister M, Lowe G, Berg HC. 1987. The proton flux through the bacterial flagellar motor. *Cell* 49:643–650. [https://doi.org/10.1016/0092-8674\(87\)90540-x](https://doi.org/10.1016/0092-8674(87)90540-x).
- Atsumi T, McCarter L, Imae Y. 1992. Polar and lateral flagellar motors of marine *Vibrio* are driven by different ion-motive forces. *Nature* 355:182–184. <https://doi.org/10.1038/355182a0>.
- Samatey FA, Imada K, Nagashima S, Vonderviszt F, Kumasaka T, Yamamoto M, Namba K. 2001. Structure of the bacterial flagellar protofilament and implications for a switch for supercoiling. *Nature* 410:331–337. <https://doi.org/10.1038/35066504>.
- Berg HC. 2000. Constraints on models for the flagellar rotary motor. *Philos Trans R Soc Lond B Biol Sci* 355:491–501. <https://doi.org/10.1098/rstb.2000.0590>.
- Feklistov A, Darst SA. 2011. Structural basis for promoter-10 element recognition by the bacterial RNA polymerase sigma subunit. *Cell* 147:1257–1269. <https://doi.org/10.1016/j.cell.2011.10.041>.
- Shi W, Zhou W, Zhang B, Huang S, Jiang Y, Schammel A, Hu Y, Liu B. 2020. Structural basis of bacterial sigma(28)-mediated transcription reveals roles of the RNA polymerase zinc-binding domain. *EMBO J* 39:e104389. <https://doi.org/10.15252/emboj.2020104389>.
- Chadsey MS, Hughes KT. 2001. A multipartite interaction between *Salmonella* transcription factor sigma28 and its anti-sigma factor FlgM: implications for sigma28 holoenzyme destabilization through stepwise binding. *J Mol Biol* 306:915–929. <https://doi.org/10.1006/jmbi.2001.4438>.
- Hughes KT, Gillen KL, Semon MJ, Karlinsky JE. 1993. Sensing structural intermediates in bacterial flagellar assembly by export of a negative regulator. *Science* 262:1277–1280. <https://doi.org/10.1126/science.8235660>.
- Helmann JD. 2019. Where to begin? Sigma factors and the selectivity of transcription initiation in bacteria. *Mol Microbiol* 112:335–347. <https://doi.org/10.1111/mmi.14309>.
- Wosten MM, van Dijk L, Veenendaal AK, de Zoete MR, Bleumink-Pluijm NM, van Putten JP. 2010. Temperature-dependent FlgM/FliA complex formation regulates *Campylobacter jejuni* flagella length. *Mol Microbiol* 75:1577–1591. <https://doi.org/10.1111/j.1365-2958.2010.07079.x>.
- Colland F, Rain JC, Gounon P, Labigne A, Legrain P, De Reuse H. 2001. Identification of the *Helicobacter pylori* anti-sigma28 factor. *Mol Microbiol* 41:477–487. <https://doi.org/10.1046/j.1365-2958.2001.02537.x>.
- Josenshans C, Niehus E, Amersbach S, Horster A, Betz C, Drescher B, Hughes KT, Suerbaum S. 2002. Functional characterization of the antagonistic flagellar late regulators FliA and FlgM of *Helicobacter pylori* and their effects on the *H. pylori* transcriptome. *Mol Microbiol* 43:307–322. <https://doi.org/10.1046/j.1365-2958.2002.02765.x>.
- Potvin E, Sanschagrin F, Levesque RC. 2008. Sigma factors in *Pseudomonas aeruginosa*. *FEMS Microbiol Rev* 32:38–55. <https://doi.org/10.1111/j.1574-6976.2007.00092.x>.
- Prouty MG, Correa NE, Klose KE. 2001. The novel sigma54- and sigma28-dependent flagellar gene transcription hierarchy of *Vibrio cholerae*. *Mol Microbiol* 39:1595–1609. <https://doi.org/10.1046/j.1365-2958.2001.02348.x>.
- Chen YF, Helmann JD. 1992. Restoration of motility to an *Escherichia coli* fliA flagellar mutant by a *Bacillus subtilis* sigma factor. *Proc Natl Acad Sci U S A* 89:5123–5127. <https://doi.org/10.1073/pnas.89.11.5123>.
- Eichelberg K, Galan JE. 2000. The flagellar sigma factor FliA (sigma(28)) regulates the expression of *Salmonella* genes associated with the centisome 63 type III secretion system. *Infect Immun* 68:2735–2743. <https://doi.org/10.1128/IAI.68.5.2735-2743.2000>.
- Heuner K, Dietrich C, Skriwan C, Steinert M, Hacker J. 2002. Influence of the alternative sigma(28) factor on virulence and flagellum expression of *Legionella pneumophila*. *Infect Immun* 70:1604–1608. <https://doi.org/10.1128/IAI.70.3.1604-1608.2002>.
- Lertsethtakarn P, Ottemann KM, Hendrixson DR. 2011. Motility and chemotaxis in *Campylobacter* and *Helicobacter*. *Annu Rev Microbiol* 65:389–410. <https://doi.org/10.1146/annurev-micro-090110-102908>.
- Kutsukake K, Iino T. 1994. Role of the FliA-FlgM regulatory system on the transcriptional control of the flagellar regulon and flagellar formation in *Salmonella typhimurium*. *J Bacteriol* 176:3598–3605. <https://doi.org/10.1128/jb.176.12.3598-3605.1994>.
- Radolf JD, Deka RK, Anand A, Smajs D, Norgard MV, Yang XF. 2016. *Treponema pallidum*, the syphilis spirochete: making a living as a stealth pathogen. *Nat Rev Microbiol* 14:744–759. <https://doi.org/10.1038/nrmicro.2016.141>.
- Rosa PA, Tilly K, Stewart PE. 2005. The burgeoning molecular genetics of the Lyme disease spirochaete. *Nat Rev Microbiol* 3:129–143. <https://doi.org/10.1038/nrmicro1086>.
- Picardeau M. 2017. Virulence of the zoonotic agent of leptospirosis: still terra incognita? *Nat Rev Microbiol* 15:297–307. <https://doi.org/10.1038/nrmicro.2017.5>.
- Holt SC, Ebersole JL. 2005. *Porphyromonas gingivalis*, *Treponema denticola*, and *Tannerella forsythia*: the “red complex,” a prototype polybacterial pathogenic consortium in periodontitis. *Periodontol* 2000 38:72–122. <https://doi.org/10.1111/j.1600-0757.2005.00113.x>.
- Li C, Motaleb A, Sal M, Goldstein SF, Charon NW. 2000. Spirochete periplasmic flagella and motility. *J Mol Microbiol Biotechnol* 2:345–354.
- Charon NW, Cockburn A, Li C, Liu J, Miller KA, Miller MR, Motaleb MA, Wolgemuth CW. 2012. The unique paradigm of spirochete motility and chemotaxis. *Annu Rev Microbiol* 66:349–370. <https://doi.org/10.1146/annurev-micro-092611-150145>.
- San Martin F, Fule L, Iraola G, Buschiazio A, Picardeau M. 2022. Diving into the complexity of the spirochetal endoflagellum. *Trends Microbiol* <https://doi.org/10.1016/j.tim.2022.09.010>.
- Zhang K, He J, Cantalano C, Guo Y, Liu J, Li C. 2020. FlhF regulates the number and configuration of periplasmic flagella in *Borrelia burgdorferi*. *Mol Microbiol* 113:1122–1139. <https://doi.org/10.1111/mmi.14482>.
- Sze CW, Morado DR, Liu J, Charon NW, Xu H, Li C. 2011. Carbon storage regulator A (CsrA(Bb)) is a repressor of *Borrelia burgdorferi* flagellin protein FlaB. *Mol Microbiol* 82:851–864. <https://doi.org/10.1111/j.1365-2958.2011.07853.x>.
- Wolgemuth CW. 2015. Flagellar motility of the pathogenic spirochetes. *Semin Cell Dev Biol* 46:104–112. <https://doi.org/10.1016/j.semcdb.2015.10.015>.
- Motaleb MA, Liu J, Wooten RM. 2015. Spirochetal motility and chemotaxis in the natural enzootic cycle and development of Lyme disease. *Curr Opin Microbiol* 28:106–113. <https://doi.org/10.1016/j.mib.2015.09.006>.
- Zhao X, Zhang K, Boquoi T, Hu B, Motaleb MA, Miller KA, James ME, Charon NW, Manson MD, Norris SJ, Li C, Liu J. 2013. Cryoelectron tomography reveals the sequential assembly of bacterial flagella in *Borrelia burgdorferi*. *Proc Natl Acad Sci U S A* 110:14390–14395. <https://doi.org/10.1073/pnas.1308306110>.

36. Chang Y, Xu H, Motaleb MA, Liu J. 2021. Characterization of the flagellar collar reveals structural plasticity essential for spirochete motility. *mBio* 12:e02494-21. <https://doi.org/10.1128/mBio.02494-21>.
37. Moon KH, Zhao X, Xu H, Liu J, Motaleb MA. 2018. A tetratricopeptide repeat domain protein has profound effects on assembly of periplasmic flagella, morphology and motility of the Lyme disease spirochete *Borrelia burgdorferi*. *Mol Microbiol* 110:634–647. <https://doi.org/10.1111/mmi.14121>.
38. Moon KH, Zhao X, Manne A, Wang J, Yu Z, Liu J, Motaleb MA. 2016. Spirochetes flagellar collar protein FlbB has astounding effects in orientation of periplasmic flagella, bacterial shape, motility, and assembly of motors in *Borrelia burgdorferi*. *Mol Microbiol* 102:336–348. <https://doi.org/10.1111/mmi.13463>.
39. Lynch MJ, Miller M, James M, Zhang S, Zhang K, Li C, Charon NW, Crane BR. 2019. Structure and chemistry of lysinoalanine crosslinking in the spirochaete flagella hook. *Nat Chem Biol* 15:959–965. <https://doi.org/10.1038/s41589-019-0341-3>.
40. Miller MR, Miller KA, Bian J, James ME, Zhang S, Lynch MJ, Callery PS, Hettick JM, Cockburn A, Liu J, Li C, Crane BR, Charon NW. 2016. Spirochaete flagella hook proteins self-catalyze a lysinoalanine covalent crosslink for motility. *Nat Microbiol* 1:16134. <https://doi.org/10.1038/nmicrobiol.2016.134>.
41. Kurniyati K, Chang Y, Liu J, Li C. 2022. Transcriptional and functional characterizations of multiple flagellin genes in spirochetes. *Mol Microbiol* 118:175–190. <https://doi.org/10.1111/mmi.14959>.
42. Kurniyati K, Kelly JF, Vinogradov E, Robotham A, Tu Y, Wang J, Liu J, Logan SM, Li C. 2017. A novel glycan modifies the flagellar filament proteins of the oral bacterium *Treponema denticola*. *Mol Microbiol* 103:67–85. <https://doi.org/10.1111/mmi.13544>.
43. Norris SJ, Charon NW, Cook RG, Fuentes MD, Limberger RJ. 1988. Antigenic relatedness and N-terminal sequence homology define two classes of periplasmic flagellar proteins of *Treponema pallidum* subsp. *pallidum* and *Treponema phagedenis*. *J Bacteriol* 170:4072–4082. <https://doi.org/10.1128/jb.170.9.4072-4082.1988>.
44. Li C, Sal M, Marko M, Charon NW. 2010. Differential regulation of the multiple flagellins in spirochetes. *J Bacteriol* 192:2596–2603. <https://doi.org/10.1128/JB.01502-09>.
45. Li C, Wolgemuth CW, Marko M, Morgan DG, Charon NW. 2008. Genetic analysis of spirochete flagellin proteins and their involvement in motility, filament assembly, and flagellar morphology. *J Bacteriol* 190:5607–5615. <https://doi.org/10.1128/JB.00319-08>.
46. Wunder EA, Jr, Slamti I, Suwondo DN, Gibson KH, Shang Z, Sindelar CV, Trajtenberg F, Buschiazio A, Ko AI, Picardeau M. 2018. FcpB is a surface filament protein of the endoflagellum required for the motility of the spirochete *Leptospira*. *Front Cell Infect Microbiol* 8:130. <https://doi.org/10.3389/fcimb.2018.00130>.
47. Gibson KH, Trajtenberg F, Wunder EA, Brady MR, San Martin F, Mechaly A, Shang Z, Liu J, Picardeau M, Ko A, Buschiazio A, Sindelar CV. 2020. An asymmetric sheath controls flagellar supercoiling and motility in the *Leptospira* spirochete. *eLife* 9:e53672. <https://doi.org/10.7554/eLife.53672>.
48. Kurniyati K, Chang Y, Liu J, Li C. 2022. Identification and characterization of the alternative sigma(28) factor in *Treponema denticola*. *J Bacteriol* 204:e00248-22. <https://doi.org/10.1128/jb.00248-22>.
49. Pons T, Gonzalez B, Ceciliani F, Galizzi A. 2006. FlgM anti-sigma factors: identification of novel members of the family, evolutionary analysis, homology modeling, and analysis of sequence-structure-function relationships. *J Mol Model* 12:973–983. <https://doi.org/10.1007/s00894-005-0096-5>.
50. Sorenson MK, Ray SS, Darst SA. 2004. Crystal structure of the flagellar sigma/anti-sigma complex sigma(28)/FlgM reveals an intact sigma factor in an inactive conformation. *Mol Cell* 14:127–138. [https://doi.org/10.1016/S1097-2765\(04\)00150-9](https://doi.org/10.1016/S1097-2765(04)00150-9).
51. Daughdrill GW, Hanely LJ, Dahlquist FW. 1998. The C-terminal half of the anti-sigma factor FlgM contains a dynamic equilibrium solution structure favoring helical conformations. *Biochemistry* 37:1076–1082. <https://doi.org/10.1021/bi971952t>.
52. Zhao M, Zhang H, Liu G, Wang L, Wang J, Gao Z, Dong Y, Zhang L, Gong Y. 2016. Structural insights into the methylation of C1402 in 16S rRNA by methyltransferase RsmI. *PLoS One* 11:e0163816. <https://doi.org/10.1371/journal.pone.0163816>.
53. Iyoda S, Kutsukake K. 1995. Molecular dissection of the flagellum-specific anti-sigma factor, FlgM, of *Salmonella typhimurium*. *Mol Gen Genet* 249:417–424. <https://doi.org/10.1007/BF00287103>.
54. Chang Y, Zhang K, Carroll BL, Zhao X, Charon NW, Norris SJ, Motaleb MA, Li C, Liu J. 2020. Molecular mechanism for rotational switching of the bacterial flagellar motor. *Nat Struct Mol Biol* 27:1041–1047. <https://doi.org/10.1038/s41594-020-0497-2>.
55. Wozniak CE, Hughes KT. 2008. Genetic dissection of the consensus sequence for the class 2 and class 3 flagellar promoters. *J Mol Biol* 379:936–952. <https://doi.org/10.1016/j.jmb.2008.04.043>.
56. Barembruch C, Hengge R. 2007. Cellular levels and activity of the flagellar sigma factor FlIA of *Escherichia coli* are controlled by FlgM-modulated proteolysis. *Mol Microbiol* 65:76–89. <https://doi.org/10.1111/j.1365-2958.2007.05770.x>.
57. Kurniyati K, Liu J, Zhang JR, Min Y, Li C. 2019. A pleiotropic role of FlaG in regulating the cell morphogenesis and flagellar homeostasis at the cell poles of *Treponema denticola*. *Cell Microbiol* 21:e12886. <https://doi.org/10.1111/cmi.12886>.
58. Mukherjee S, Yakhnin H, Kysela D, Sokoloski J, Babitzke P, Kearns DB. 2011. CsrA-FlhW interaction governs flagellin homeostasis and a checkpoint on flagellar morphogenesis in *Bacillus subtilis*. *Mol Microbiol* 82:447–461. <https://doi.org/10.1111/j.1365-2958.2011.07822.x>.
59. Dugar G, Svensson SL, Bischler T, Waldchen S, Reinhardt R, Sauer M, Sharma CM. 2016. The CsrA-FlhW network controls polar localization of the dual-function flagellin mRNA in *Campylobacter jejuni*. *Nat Commun* 7:11667. <https://doi.org/10.1038/ncomms11667>.
60. Potts AH, Vakulskas CA, Pannuri A, Yakhnin H, Babitzke P, Romeo T. 2017. Global role of the bacterial post-transcriptional regulator CsrA revealed by integrated transcriptomics. *Nat Commun* 8:1596. <https://doi.org/10.1038/s41467-017-01613-1>.
61. Seshadri R, Myers GS, Tettelin H, Eisen JA, Heidelberg JF, Dodson RJ, Davidsen TM, DeBoy RT, Fouts DE, Haft DH, Selengut J, Ren Q, Brinkac LM, Madupu R, Kolonay J, Durkin SA, Daugherty SC, Shetty J, Shvartsbeyn A, Gebregeorgis E, Geer K, Tsegaye G, Malek J, Ayodeji B, Shatsman S, McLeod MP, Smajs D, Howell JK, Pal S, Amin A, Vashisth P, McNeill TZ, Xiang Q, Sodergren E, Baca E, Weinstock GM, Norris SJ, Fraser CM, Paulsen IT. 2004. Comparison of the genome of the oral pathogen *Treponema denticola* with other spirochete genomes. *Proc Natl Acad Sci U S A* 101:5646–5651. <https://doi.org/10.1073/pnas.0307639101>.
62. Ding L, Wang Y, Hu Y, Atkinson S, Williams P, Chen S. 2009. Functional characterization of FlgM in the regulation of flagellar synthesis and motility in *Yersinia pseudotuberculosis*. *Microbiology (Reading)* 155:1890–1900. <https://doi.org/10.1099/mic.0.026294.0>.
63. Caramori T, Barilla D, Nessi C, Sacchi L, Galizzi A. 1996. Role of FlgM in sigma D-dependent gene expression in *Bacillus subtilis*. *J Bacteriol* 178:3113–3118. <https://doi.org/10.1128/jb.178.11.3113-3118.1996>.
64. Correa NE, Barker JR, Klose KE. 2004. The *Vibrio cholerae* FlgM homologue is an anti-sigma28 factor that is secreted through the sheathed polar flagellum. *J Bacteriol* 186:4613–4619. <https://doi.org/10.1128/JB.186.14.4613-4619.2004>.
65. Bian J, Li C. 2011. Disruption of a type II endonuclease (TDE0911) enables *Treponema denticola* ATCC 35405 to accept an unmethylated shuttle vector. *Appl Environ Microbiol* 77:4573–4578. <https://doi.org/10.1128/AEM.00417-11>.
66. Chi B, Chauhan S, Kuramitsu H. 1999. Development of a system for expressing heterologous genes in the oral spirochete *Treponema denticola* and its use in expression of the *Treponema pallidum* flaA gene. *Infect Immun* 67:3653–3656. <https://doi.org/10.1128/IAI.67.7.3653-3656.1999>.
67. Jutras BL, Scott M, Parry B, Biboy J, Gray J, Vollmer W, Jacobs-Wagner C. 2016. Lyme disease and relapsing fever *Borrelia* elongate through zones of peptidoglycan synthesis that mark division sites of daughter cells. *Proc Natl Acad Sci U S A* 113:9162–9170. <https://doi.org/10.1073/pnas.1610805113>.
68. Fraser CM, Norris SJ, Weinstock GM, White O, Sutton GG, Dodson R, Gwinn M, Hickey EK, Clayton R, Ketchum KA, Sodergren E, Hardham JM, McLeod MP, Salzberg S, Peterson J, Khalak H, Richardson D, Howell JK, Chidambaram M, Utterback T, McDonald L, Artiach P, Bowman C, Cotton MD, Fujii C, Garland S, Hatch B, Horst K, Roberts K, Sandusky M, Weidman J, Smith HO, Venter JC. 1998. Complete genome sequence of *Treponema pallidum*, the syphilis spirochete. *Science* 281:375–388. <https://doi.org/10.1126/science.281.5375.375>.
69. Balaban M, Joslin SN, Hendrixson DR. 2009. FlhF and its GTPase activity are required for distinct processes in flagellar gene regulation and biosynthesis in *Campylobacter jejuni*. *J Bacteriol* 191:6602–6611. <https://doi.org/10.1128/JB.00884-09>.
70. Kusumoto A, Shinohara A, Terashima H, Kojima S, Yakushi T, Homma M. 2008. Collaboration of FlhF and FlhG to regulate polar-flagella number and localization in *Vibrio alginolyticus*. *Microbiology (Reading)* 154:1390–1399. <https://doi.org/10.1099/mic.0.2007/012641-0>.
71. Park S, Yoon J, Lee CR, Lee JY, Kim YR, Jang KS, Lee KH, Seok YJ. 2019. Polar landmark protein HubP recruits flagella assembly protein FapA under glucose limitation in *Vibrio vulnificus*. *Mol Microbiol* 112:266–279. <https://doi.org/10.1111/mmi.14268>.

72. Park S, Park YH, Lee CR, Kim YR, Seok YJ. 2016. Glucose induces delocalization of a flagellar biosynthesis protein from the flagellated pole. *Mol Microbiol* 101:795–808. <https://doi.org/10.1111/mmi.13424>.
73. Ohta K, Makinen KK, Loesche WJ. 1986. Purification and characterization of an enzyme produced by *Treponema denticola* capable of hydrolyzing synthetic trypsin substrates. *Infect Immun* 53:213–220. <https://doi.org/10.1128/iai.53.1.213-220.1986>.
74. Ruby JD, Li H, Kuramitsu H, Norris SJ, Goldstein SF, Buttle KF, Charon NW. 1997. Relationship of *Treponema denticola* periplasmic flagella to irregular cell morphology. *J Bacteriol* 179:1628–1635. <https://doi.org/10.1128/jb.179.5.1628-1635.1997>.
75. Kurniyati K, Li C. 2016. *pyrF* as a counterselectable marker for unmarked genetic manipulations in *Treponema denticola*. *Appl Environ Microbiol* 82:1346–1352. <https://doi.org/10.1128/AEM.03704-15>.
76. Li H, Ruby J, Charon N, Kuramitsu H. 1996. Gene inactivation in the oral spirochete *Treponema denticola*: construction of an *flgE* mutant. *J Bacteriol* 178:3664–3667. <https://doi.org/10.1128/jb.178.12.3664-3667.1996>.
77. Kurniyati K, Li C. 2021. Genetic manipulations of oral spirochete *Treponema denticola*. *Methods Mol Biol* 2210:15–23. https://doi.org/10.1007/978-1-0716-0939-2_2.
78. Oshiro RT, Rajendren S, Hundley HA, Kearns DB. 2019. Robust stoichiometry of *FliW-CsrA* governs flagellin homeostasis and cytoplasmic organization in *Bacillus subtilis*. *mBio* 10:e00533-19. <https://doi.org/10.1128/mBio.00533-19>.
79. Limberger RJ, Slivienski LL, Izard J, Samsonoff WA. 1999. Insertional inactivation of *Treponema denticola* *tap1* results in a nonmotile mutant with elongated flagellar hooks. *J Bacteriol* 181:3743–3750. <https://doi.org/10.1128/JB.181.12.3743-3750.1999>.
80. Orth R, O'Brien-Simpson N, Dashper S, Walsh K, Reynolds E. 2010. An efficient method for enumerating oral spirochetes using flow cytometry. *J Microbiol Methods* 80:123–128. <https://doi.org/10.1016/j.mimet.2009.11.006>.
81. Mastronarde DN. 2005. Automated electron microscope tomography using robust prediction of specimen movements. *J Struct Biol* 152:36–51. <https://doi.org/10.1016/j.jsb.2005.07.007>.
82. Kremer JR, Mastronarde DN, McIntosh JR. 1996. Computer visualization of three-dimensional image data using IMOD. *J Struct Biol* 116:71–76. <https://doi.org/10.1006/jsbi.1996.0013>.
83. Webb B, Sali A. 2016. Comparative protein structure modeling using MODELLER. *Curr Protoc Bioinformatics* 54:5.6.1–5.6.37. <https://doi.org/10.1002/cpbi.3>.
84. Zimmermann L, Stephens A, Nam SZ, Rau D, Kubler J, Lozajic M, Gabler F, Soding J, Lupas AN, Alva V. 2018. A completely reimplemented MPI Bioinformatics Toolkit with a new HHpred server at its core. *J Mol Biol* 430:2237–2243. <https://doi.org/10.1016/j.jmb.2017.12.007>.
85. Kozakov D, Hall DR, Xia B, Porter KA, Padhorney D, Yueh C, Beglov D, Vajda S. 2017. The ClusPro web server for protein-protein docking. *Nat Protoc* 12:255–278. <https://doi.org/10.1038/nprot.2016.169>.
86. Wolfe AJ, Berg HC. 1989. Migration of bacteria in semisolid agar. *Proc Natl Acad Sci U S A* 86:6973–6977. <https://doi.org/10.1073/pnas.86.18.6973>.